

## Supplementary Material

### The melting profile

To measure the melting curves of DNA by spatially scanning the thermal profile, we assumed that the DNA was at thermal equilibrium at each point of space. This assumption is true if thermal equilibration is fast compared to the drift and diffusion velocity. The drift can originate from the electrophoretic mobility of the DNA or its convection in a electroosmotic flow (if present). Because we use AC voltages the average value of the drift is zero. Notice that most of the melting profile is measured outside the hole region where the electric field is small; only the small  $z$ -values correspond to the vicinity of the hole where the field is appreciable. The excursion of the molecule in the temperature profile during one period can be evaluated as follows. The electrophoretic mobility of DNA is largely independent on the DNA size. Its value<sup>1</sup> is  $3 \times 10^{-4}$  cm  $V^{-1}$   $s^{-1}$ . The maximum electric field can be estimated by dividing the maximum voltage by the characteristic size, that is  $E = 25/50 \times 10^{-6} = 5 \times 10^5$  V/m. The electrophoretic velocity of the DNA in the hole is then equal to  $1.5 \times 10^{-2}$  ms<sup>-1</sup>. Hence the drift distance during half a period of the field is of order 1  $\mu$ m. At larger distances from the pore the electric field decreases as  $1/r^2$  and the drift distance is correspondingly decreased.

We could not detect any electroosmotic flow. If any such drift existed it would have been localized at the hole where all flow lines converge. We used a Teflon septum in a 1M KCl solution. This means that the zeta potential and therefore the electroosmotic flow are largely reduced. The electroosmotic coefficient<sup>2</sup> for PTFE (Teflon) capillary tubing is below  $10^{-4}$   $V^{-1}$   $s^{-1}$  rendering this drift negligible.

Lastly we point out that the temperature profile is also estimated using DNA molecules with similar electrophoretic mobility and undergoing the same electroosmotic flow. Hence, the temperature that we measure at a fixed point is also the mean temperature over the excursion of the DNA in the temperature profile.

### Applicability of the device

This device can be a useful tool to produce large temperature gradients. Several parameters may affect the applicability of the concept:

1 - *AC frequency*. Heating occurs at all frequencies and increases with decreasing frequency. At small frequencies, however, the drift of the DNA molecules in one period is diminished. We tested frequencies between 1 to 30 kHz without any significant change in the results. At large enough frequencies the current across the membrane can be dominated by the capacitive charging of the membrane. The crossover frequency is  $\omega = (R_h C_s)^{-1} = ar_0^2/(\sigma C_s)^{-1}$ , where  $R_h \simeq 2300$   $\Omega$  and  $r_0$  are the pore's resistance and radius,  $C_s \simeq 0.4$  pF is the septum capacitance,  $\sigma$  is the electrical conductivity and  $a$  is a geometry-dependent factor. For the 50  $\mu$ m thick membrane we used the crossover frequency is 1 GHz. For thin membranes capacitive charging should

be considered and in this case the ion flux occurs everywhere in the solution and the heating is consequently less localized and more homogeneous. Note however that the product  $R_h C_s$  does not depend on the membrane thickness for a planar capacitor and a cylindrical hole.

2- *Buffer composition*. In the Teflon membranes we used the values of pH and salt concentration do not dramatically affect the zeta potential at the pore surface. Other polymers or solid state membrane can be affected by this parameters.

As stated above, heating occurs within a few tens of microns of the pore and the Peclet number is small. In this limit, the analysis and heating profile should be unchanged even in the presence of convection. No changes were detected in our experiments with solutions of concentrations in the range from 0.2 M to 1M.

### Numerical calculations

The governing equation for the salt concentration  $C^\pm$ , electric potential  $\phi$ , and temperature  $T$

$$\partial_t C^\pm - \nabla(D^\pm \nabla C^\pm \pm ez\mu^\pm C^\pm \nabla \phi) = 0, \quad (1)$$

$$\partial_t(\varepsilon \nabla \phi) + \nabla(\sigma \nabla \phi) = 0, \quad (2)$$

$$\rho C_p \partial_t T - \nabla(\kappa \nabla T) - \sigma(\nabla \phi)^2 = 0, \quad (3)$$

were solved using a finite element method with a high resolution mesh near the pore.  $C^\pm$ ,  $D^\pm$  and  $\mu^\pm$  are the concentration, diffusion coefficient and mobility of positive (“+”, K) and negative ions (“-”, Cl) in water, respectively. The diffusion of  $K^+$  and  $Cl^-$  ions were taken to be  $D^+ = 1.9 \times 10^{-9}$  m<sup>2</sup>/s and  $D^- = 2 \times 10^{-9}$  m<sup>2</sup>/s and the mobilities depended on the diffusion via Einstein's relation.  $e$  is the electron's charge and the valency  $z$  was chosen to be  $z = 1$ . The first equation was calculated in the aqueous region only as ions cannot penetrate the hard walls. The second equation was solved in the aqueous regions with electrical conductivity given by  $\sigma = e^2(\mu^+ C^+ + \mu^- C^-)$  and dielectric constant  $\varepsilon = 80\varepsilon_0$ , where  $\varepsilon_0$  is the vacuum permittivity, and with  $\sigma = 0$  and  $\varepsilon = 2.1\varepsilon_0$  in the solid parts. The usual boundary conditions at the interfaces between dielectric or conductive materials were used.

Due to the total electro-neutrality and the AC fields we used, convection can be neglected and the Navier-Stokes equation need not be solved. Subsequently the heat equation (third equation) has only Joule heating terms and no viscous dissipation.  $C_p$ ,  $\kappa$  and  $\rho$  are the specific heat, heat conductivity, and mass density of the aqueous region and Teflon cell. We used  $C_p = 4180$  J/Kg K<sup>o</sup>,  $\kappa = 0.58$  W/mK<sup>o</sup>, and  $\rho = 1000$  Kg/m<sup>3</sup> in water and  $C_p = 1000$  J/Kg K<sup>o</sup>,  $\kappa = 0.27$  W/mK<sup>o</sup>, and  $\rho = 2140$  Kg/m<sup>3</sup> in Teflon. At the water-Teflon interface we conserved the heat flux, and at the edges of the cell we used Newtonian heat loss to the environment (proportional to  $T - T_\infty$ ) with temperature at infinity  $T_\infty$  equal to the room temperature.

<sup>1</sup>E.Stellwagen, N.C.Stellwagen, *Electrophoresis* **23**, 2794 (2002).

<sup>2</sup>P.Camillery, *Capillary electrophoresis*, Ed: CRC Press LLC, 103 (1998).

# Localized Joule heating produced by ion current focusing through micron-size holes

V. Viasnoff,<sup>1, a)</sup> U. Bockelmann,<sup>1</sup> A. Meller,<sup>2</sup> H. Isambert,<sup>3</sup> L. Laufer,<sup>4</sup> and Y. Tsori<sup>4</sup>

<sup>1)</sup>*Nanobiophysics Lab, ESPCI, CNRS, 10 rue Vauquelin, 75005 Paris, France.*

<sup>2)</sup>*Department of Physics and Biomedical Engineering, Boston University, Boston, MA 02215, USA.*

<sup>3)</sup>*Institut Curie, CNRS, 11 rue P.M. Curie, 75005 Paris, France.*

<sup>4)</sup>*Department of Chemical Engineering, Ben-Gurion University of the Negev, 84105 Beer-Sheva, Israel.*

(Dated: 18 April 2022)

We provide an experimental demonstration that the focusing of ionic currents in a micron size hole connecting two chambers can produce local temperature increases of up to 100° C with gradients as large as 1° K $\mu\text{m}^{-1}$ . We find a good agreement between the measured temperature profiles and a finite elements-based numerical calculation. We show how the thermal gradients can be used to measure the full melting profile of DNA duplexes within a region of 40  $\mu\text{m}$ . The possibility to produce even larger gradients using sub-micron pores is discussed.

The creation of local heat sources and large thermal gradients in confined aqueous environments is a challenging problem due to the rapid diffusion of heat in water. Several solutions were proposed, such as heating micro/nanoparticles<sup>1,2</sup> by magnetic induction or by using a focused laser beam<sup>3,4</sup>. Local thermal gradients in microchannels were used to sort and concentrate molecules. Several approaches were developed such as thermophoresis<sup>5</sup>, Temperature Gradient Focusing<sup>6</sup>, Field Gradient Focusing<sup>7</sup>, and isoelectric Focusing<sup>8,9</sup>. These techniques use high DC voltages (tens to hundreds of Volts) and thermal gradients in the range of 0.01° K $\mu\text{m}^{-1}$ . The typical volumes are micro to nanoliters. In this letter, we show that a few tens of picoliters can be strongly heated by focusing an ionic current through a micron size hole in a saline solution. The resulting gradients are of the order of 1° K $\mu\text{m}^{-1}$ .

We use a custom made cell composed of two chambers separated by a 50  $\mu\text{m}$  thick Teflon septum (see Figure 1). A conical hole (40° half angle, minimum diameter  $r_0 = 7.5 \mu\text{m}$ ) is punctured in the center of the septum. The AC voltage ( $\simeq 100V_{pp}$ , 10 kHz) is applied across the chambers using platinum electrodes. We use tris buffer, 1M KCl, pH 7.4, of electrical conductance  $\sigma = 107 \text{ mS/cm}$ . The DC value of the electrical resistance  $R_h$  across the hole is 2300  $\Omega$ . The septum capacitance is estimated to  $C_s = 0.4 \text{ pF}$ . It results that the current across the chambers is mostly resistive at 10 kHz. The Joule heating power  $P_j$  dissipated in the hole is proportional to the mean root square current  $i_{\text{rms}}$ . We measure the local temperature profiles along the vertical hole axis in the lower chamber. The temperature is derived from the confocal detection ( $\lambda = 532 \text{ nm}$ ) of the calibrated fluorescence of TetraMethylRhodamine (TMR) grafted at the 5' end of DNA oligomers.

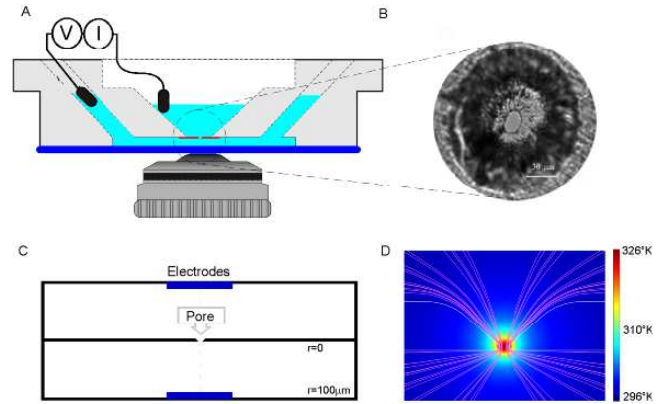


FIG. 1. A: Schematic representation of the experimental setup. The two chambers are separated by a 50  $\mu\text{m}$  thick Teflon septum punctured by a 7.5  $\mu\text{m}$  radius conical hole B: Close up on the hole region. C: Model set up used for our finite element modeling. D: close up on the pore region. The ion current lines are represented and the map of the temperature profile is color coded.

Large enough currents,  $i_{\text{rms}} > 1.9 \text{ mA}$ , result buffer vaporization. Smaller values of  $i_{\text{rms}}$  lead to stationary thermal profiles within a few seconds. Figure 2 A shows the temperature increase  $\Delta T = T - T_\infty$ , where  $T_\infty = 298^\circ\text{K}$  is the room temperature, along the vertical axis for  $i_{\text{rms}} = 1.81 \text{ mA}$ . Over the first 40  $\mu\text{m}$ , the average temperature gradient is 1° K $\mu\text{m}^{-1}$ . As a first approximation we model the heating power  $P_{\text{eff}}$  as being distributed uniformly in an effective sphere of radius  $r_{\text{eff}}$ . The temperature then reads:

$$\Delta T(r) = \frac{P_{\text{eff}}}{8\pi\kappa r_{\text{eff}}} \left( 3 - \frac{r^2}{r_{\text{eff}}^2} \right) \quad r < r_{\text{eff}}$$

$$\Delta T(r) = \frac{P_{\text{eff}}}{4\pi\kappa r} \quad r \geq r_{\text{eff}} \quad (1)$$

where  $r$  is the distance from the hole center and  $\kappa = 0.6 \text{ Wm}^{-1}\text{K}^{-1}$  is the thermal conductivity of water. Figure 2A shows the measured temperature profile for hole

<sup>a)</sup>Electronic mail: virgile.viasnoff@espci.fr

radius  $r_0 = 7.5 \mu\text{m}$  and power  $P_j = 6.5 \times 10^{-3} \text{ W}$ . The best fit parameters for our model are  $r_{\text{eff}} \simeq 17.8 \mu\text{m}$  and a  $P_{\text{eff}} = 5.2 \times 10^{-3} \text{ W}$ . This model predicts that when  $r > r_{\text{eff}}$  the value of  $(r/r_0)\Delta T(z)/\Delta T(r_0)$  is a constant independent of  $r_0$  and  $P_j$ . Figure 2B shows that the curves for several values of  $r_0$  and  $P_j$  can be scaled provided that we take  $r_{\text{eff}} = 2.4r_0$ .

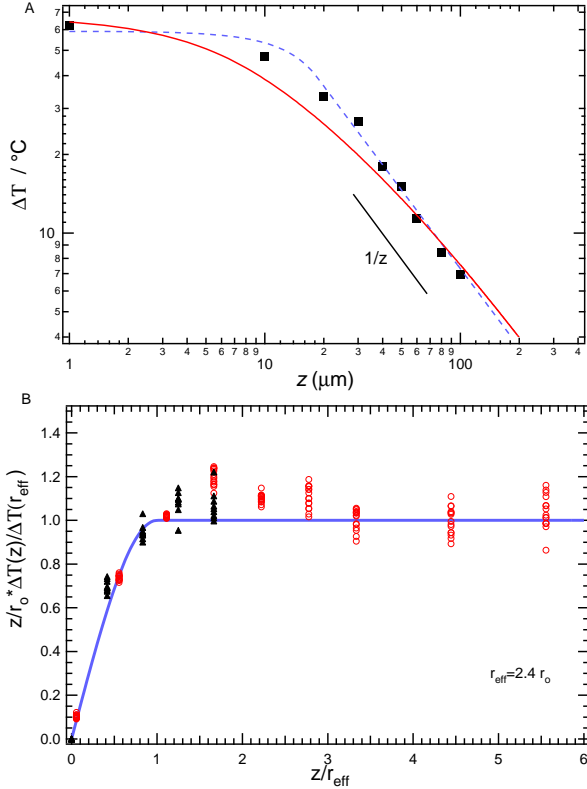


FIG. 2. A: Profile of the temperature increase  $\Delta T(z)$  along the vertical axis below the hole center. The pore's radius is  $7.5 \mu\text{m}$  and the current is  $i_{\text{rms}} = 1.81 \text{ mA}$ . The average thermal gradient over the first  $40 \mu\text{m}$  is  $1^\circ \text{ K}\mu\text{m}^{-1}$ . At distances larger than the hole radius the temperature profiles  $\Delta T(z)$  scale as  $1/z$ . The dotted line is the fit obtained when modeling the heating source by a spherical source of uniform heating power  $P_j = 5.2 \times 10^{-3} \text{ W}$  and radius  $r_{\text{eff}} = 17.8 \mu\text{m}$ . The solid line is the finite element calculation. B: Rescaling of all temperature profiles obtained with a hole of  $7.5 \mu\text{m}$  (open circles) and  $20 \mu\text{m}$  (full triangles) for various currents ( $0.5 \text{ mA} < i_{\text{rms}} < 1.85 \text{ mA}$ ). We used  $r_{\text{eff}} = 2.4 r_0$ . The straight line corresponds to the scaling of the analytical model. Inset: Values of  $\Delta T(r_{\text{eff}})$  as a function of  $I_{\text{rms}}$  for the hole of  $7.5 \mu\text{m}$  (open circles) and  $20 \mu\text{m}$  (full triangles).

In order to explore the influence of the pore geometry on thermal profiles we use a finite elements approach with various hole radiuses  $r_0$  and pore lengths  $L$ . The numerical calculation accounts for mass transport (2), electrostatic potential (3) and heat dissipation (4) in the following way:

$$\partial_t C^\pm - \nabla(D^\pm \nabla C^\pm \pm e z \mu^\pm C^\pm \nabla \phi) = 0, \quad (2)$$

$$\partial_t(\nabla(\varepsilon \nabla \phi) + \nabla(\sigma \nabla \phi)) = 0, \quad (3)$$

$$\rho C_p \partial_t T - \nabla(\kappa \nabla T) - \sigma(\nabla \phi)^2 = 0, \quad (4)$$

$C^\pm$ ,  $D^\pm$  and  $\mu^\pm$  are the number densities, the diffusion coefficients and the electrophoretic mobilities of the positive and negative ions, respectively.  $\phi$  is the electric potential,  $\varepsilon$  is the local dielectric constant,  $\sigma$  is the electrical conductivity,  $e$  is the electron's charge, and  $C_p$  is the heat capacity. The steady-state solutions were obtained with an AC voltage at the electrodes. See Supplementary Material for details.

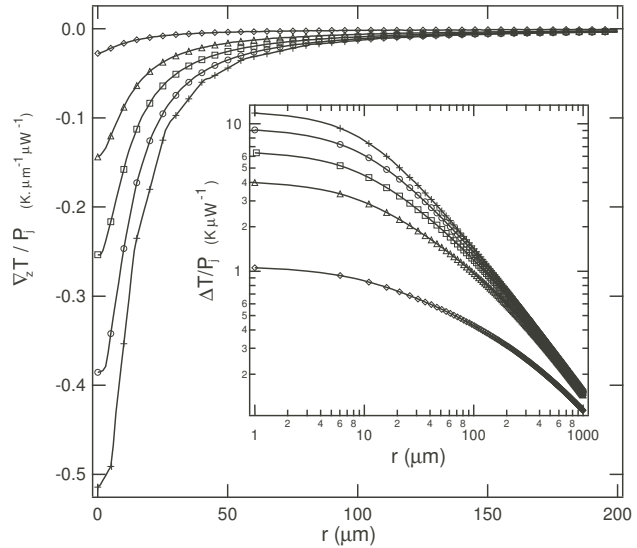


FIG. 3. Steady state temperature gradients and profiles (inset) below the narrowest constriction of the hole given by finite elements calculation.  $\nabla_z T(z)$  and  $\Delta T(z)$  are scaled by the average heating power  $P_j$  for various ratios of hole size  $r_0 = 10 \mu\text{m}$  with the membrane thickness  $L$ . The values of  $r_0/L$  are 0.01 ( $\diamond$ ), 0.05 ( $\triangle$ ), 0.1 ( $\square$ ), 0.2 ( $\circ$ ), 0.5 ( $+$ ).  $\Delta T(z)$  agrees with Eq. 1 and decays like  $z^{-1}$  at  $z > r_0$  for  $r_0/L$  larger than 0.1. For lower ratios the thermal gradients are less steep.

Figure 3 shows the calculated temperature  $\Delta T(z)$  and gradient profiles  $\nabla_z T(z)$  along the  $z$  axis at a fixed heating power  $P_j$  for several values of the aspect ratio  $r_0/L$ . When  $r_0/L > 0.1$  the temperature is well described by  $\Delta T(z) \sim z^{-1}$  for  $z$  values larger than  $2r_0$ . In the limit of small aspect ratio the heating is mainly localized in the hole and smoothly spreads in the lower chamber producing smaller temperature gradients. We conclude that  $r_0/L$  should ideally be between 0.1 and 1 to obtain the sharpest gradients and largest temperature increases.

The experimental thermal gradients generated by a hole of diameter  $r_0 = 20 \mu\text{m}$  are used to determine the melting profile a DNA duplex: strand 1: TMR 5'-TCAGACCG(TC)<sub>15</sub>-3', strand 2: 5'-CGGTCTGA-3' IowaBlack. The DNA was gel purified to obtain a 95% hybridization efficiency. The fluorescence intensity of the TMR is quenched 20-fold on average upon

hybridization with IowaBlack. With a proper baseline calibration the fluorescence intensity measured at the laser spot can be used to determine the fraction of hybridized duplexes. We measure the fluorescence profiles at various values of  $i_{\text{rms}}$  for strand 1 only, and for the hybridized duplex with a 1:1 ratio of both strands (see Figure 4). Assuming (i) a local thermal equilibrium, (ii) a two state model where the 8 mers are either fully hybridized or completely open, and (iii) an efficient quenching for all temperatures, we can extract the dissociation coefficient  $\alpha$  of the hairpin as a function of temperature and distance from the pore. Figure 4 shows the full melting profile obtained over a distance of 45  $\mu\text{m}$  for a hole of radius  $r_0 = 20 \mu\text{m}$ . Following the typical melting curve analysis for bimolecular equilibrium<sup>10</sup>, we extract the thermodynamical parameters of the DNA structure. We find  $\Delta H = -66 \pm 6 \text{ kCal mole}^{-1}$  and  $\Delta S = 182 \pm 25 \text{ Cal mole}^{-1} \text{ K}^{-1}$ , in good agreement with the thermodynamical parameters calculated with MFold<sup>11</sup> under similar salt conditions ( $\Delta H = -62 \text{ kCal mole}^{-1}$  and  $\Delta S = 169 \text{ Cal mole}^{-1} \text{ K}^{-1}$ ). Spatial temperature gradients have the advantage over traditional melting curves techniques that all temperatures can be probed simultaneously. This method works if the diffusion and/or drift of the DNA molecule across the thermal profile is slow enough to allow thermal equilibration. As derived in the Supplementary Material, electrophoretic and electroosmotic drifts are negligible in our experiments. The Brownian diffusion coefficient<sup>12</sup> for our DNA molecules is of order  $D_{\text{DNA}} \simeq 10^{-7} \text{ cm}^2 \text{ s}^{-1}$ . The distance over which the temperature changes by  $1^\circ\text{C}$  is  $d=1 \mu\text{m}$ . The diffusion time across this distance is  $\tau = d^2/D_{\text{DNA}} = 0.01 \text{ s}$ . Since small molecular beacons are reported to open over a characteristic time of  $10^{-4} \text{ s}$ <sup>13</sup>, the approximation of local equilibrium is satisfied.

We briefly discuss the influence of various parameters on the applicability of our device. For frequencies  $\omega < (R_h C_s)^{-1} = ar_0^2/(\sigma C_s)$ , where  $a$  is a geometry-dependent factor, the ionic current is mostly resistive. It is reasonable to assume that electroosmotic flow are negligible due to the use of AC fields. Electroosmosis can be significantly enhanced in smaller ( $\simeq 100 \text{ nm}$ ) or charged pores when current rectification occurs<sup>14</sup>. In the lower chamber natural convection is minimized since the hot spot (the hole) is located above the cold region. In addition, there is negligible fluid transfer between the upper and lower chambers. The small extent of the lower chamber also increases the instability threshold for natural convection. This situation contrasts with focused laser heating for which convective rolls are observed along the optical axis<sup>4</sup>. Convection can be externally applied to drive the molecule through the thermal profile. Our conclusions would still hold in

the limit of small Peclet numbers i.e if the convective velocity is small:  $v < \kappa/\rho C_p r_0 = 10^{-5}/r_0 \text{ m s}^{-1}$ . In this limit thermal quenching rate of  $1^\circ \text{ K}/\mu\text{s}$  can still

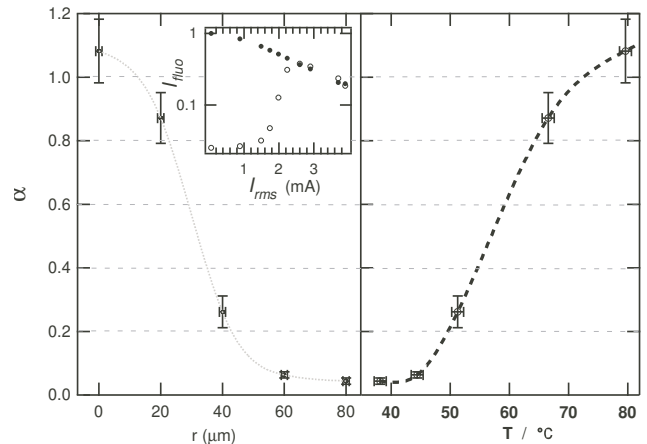


FIG. 4. The dissociation ratio  $\alpha \equiv I_{\text{fluo}}(\text{DNA} + \text{quencher})/I_{\text{fluo}}(\text{DNA only})$  as a function of distance and temperature for  $i_{\text{rms}} = 2.9 \text{ mA}$ . A decrease of 90% is obtained over 45  $\mu\text{m}$  or  $35^\circ\text{C}$ . The hole diameter is 40  $\mu\text{m}$ . Inset: fluorescence intensity as a function of the ionic current for a single DNA strand labeled with TMR only (full symbol) and a DNA duplex with TMR quenched with IowaBlack (open symbol). The lines are guides to the eyes.

be achieved. See Supplementary Material for a detailed discussion. We believe that this approach facilitates the creation of large thermal gradients in sub-micron regions with potential applications for fast denaturation and thermal quenching<sup>15</sup> to study local chemical reactions.

- <sup>1</sup>K. Hamad-Schifferli, J. J. Schwartz, A. T. Santos, S. G. Zhang, and J. M. Jacobson, *Nature* **415**, 152 (2002).
- <sup>2</sup>M. Levy, C. Wilhelm, J. M. Siaugue, O. Horner, J. C. Bacri, and F. Gazeau, *J. Phys-Condens. Mat.* **20**, 204133 (2008).
- <sup>3</sup>P. Baaske, S. Duhr, and D. Braun, *Appl. Phys. Lett.* **91**, 133901 (2007).
- <sup>4</sup>D. Braun and A. Libchaber, *Phys. Rev. Lett.* **89**, 188103 (2002).
- <sup>5</sup>S. Duhr and D. Braun, *Proc. Natl. Acad. Sci. U.S.A.* **103**, 19678 (2006).
- <sup>6</sup>D. Ross and L. E. Locascio, *Anal. Chem.* **74**, 2556 (2002).
- <sup>7</sup>W. S. Koegler and C. F. Ivory, *Biotechnol. Progr.* **12**, 822 (1996).
- <sup>8</sup>J. Pawliszyn and J. Q. Wu, *J. Microcolumn. Sep.* **5**, 397 (1993).
- <sup>9</sup>B. Kates and C. L. Ren, *Electrophoresis* **27**, 1967 (2006).
- <sup>10</sup>J. L. Mergny and L. Lacroix, *Oligonucleotides* **13**, 515 (2003).
- <sup>11</sup><http://www.bioinfo.rpi.edu/applications/mfold>.
- <sup>12</sup>B. Tinland, A. Pluen, J. Sturm, and G. Weill, *Macromolecules* **30**, 5763 (1997).
- <sup>13</sup>G. Bonnet, O. Krichevsky, and A. Libchaber, *Proc. Natl. Acad. Sci. U.S.A.* **95**, 8602 (1998).
- <sup>14</sup>Z. Siwy, *Adv. Funct. Mat.* **16**, 735 (2002).
- <sup>15</sup>V. Viasnoff, A. Meller, and H. Isambert, *Nano.Letters* **6**, 101 (2006).